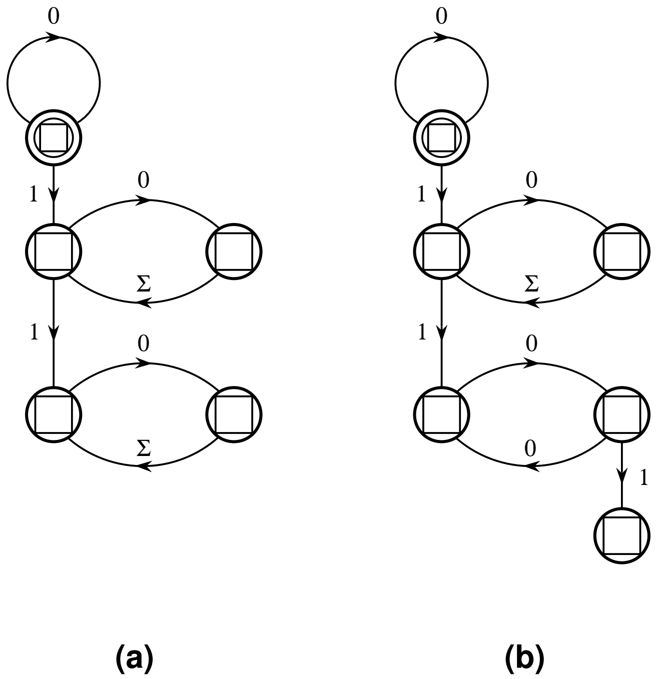

(a) **(b)**

Fig. 10.13 Machines reconstructed from a CA state on a lattice of size $N = 10^5$, evolving under ECA 18 from a random initial condition. (a) at time $t = 100,000$; (b) at time $t = 100,001$. Both reconstructions were performed with tree depth $D = 8$ and morph depth $L = 4$.

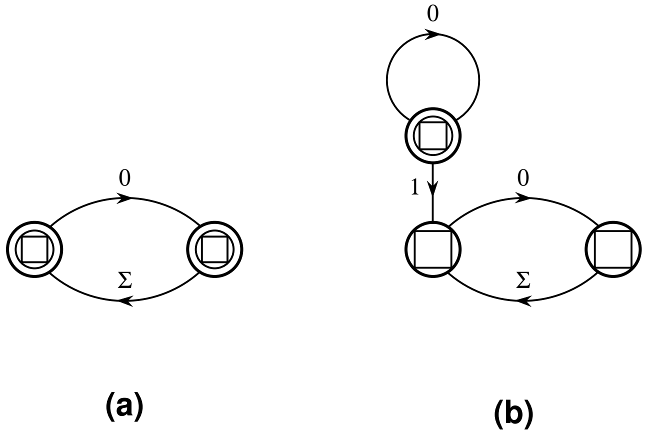

(a) **(b)**

Fig. 10.14 ECA 18 domain. (a) The process graph of Λ^0 in which both states are start and final states. The symbol Σ denotes the symbol set $\{0, 1\}$. (b) The minimal DFA for Λ^0. Both machines accept exactly the same set of strings.

10.13(b), which show the machines reconstructed at tree depth $D = 8$ and morph depth $L = 4$ from $\mathrm{s}_{100,000}$ and $\mathrm{s}_{100,001}$, respectively. The variations consisted of missing edges or nondeterministic transitions to "dangling" states from which there was no exiting edge, both of which are common signatures of incomplete statistics. The recurrent components were then excised from the reconstructed machines and tested for invariance.

By this means we found the domain language Λ^0_{18}, with process graph shown in fig. 10.14(a), and minimal DFA shown in fig. 10.14(b). The DFA differs from the process graph by having a unique start state devoted to synchronization of the machine. The sets of strings accepted by the two machines are identical. It is evident that Λ^0_{18} faithfully captures the "every other cell is 0" pattern mentioned above. The empirical realization was that Λ^0_{18} is a trapping set, i.e., that the iterates of Λ^0_{18} remain in Λ^0_{18} forever. What was not known, however, was whether this set was invariant, or whether there were additional restrictions, so that iterates of Λ^0_{18} fell into some proper subset of Λ^0_{18}. This question could only be answered by some analytic technique such as the FME algorithm.

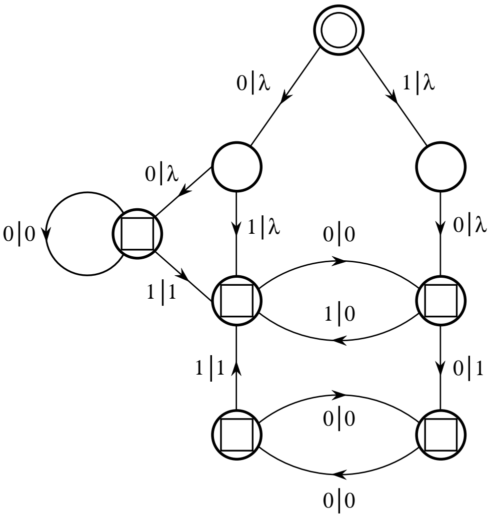

Fig. 10.15 Λ^0_{18} is a regular domain: Machine $\mathrm{T}_{18} \circ \mathrm{M}(\Lambda^0_{18})$ obtained after composing the ECA 18 update transducer with the domain machine of fig. 10.14(b). Minimization with respect to the output results in a machine identical to that shown in fig. 10.14(b).

Proposition. Λ^0_{18} is a regular domain of ECA 18.

Proof: (i) Temporal invariance: by explicit construction using the FME algorithm. To illustrate the FME algorithm, we go into a little more detail in proving the invariance of Λ^0_{18}. Fig. 10.15 shows an intermediate stage of the construction of the first iterate of $\mathrm{M}(\Lambda^0_{18})$, immediately after composing the machine with the ECA 18 update transducer T_{18}. After minimizing with respect to the output, the final machine $\mathrm{M}(\mathrm{T}_{18}\Lambda^0_{18}) = [\mathrm{T}_{18} \circ \mathrm{M}(\Lambda^0_{18})]_{\mathrm{out}}$ is seen to be identical to $\mathrm{M}(\Lambda^0_{18})$. (ii) Spatial homogeneity: this follows immediately since the process graph of Λ^0_{18}, shown in fig. 10.14(a), is strongly connected. ▌

The domain transducer $\mathrm{T}_{\Lambda^0_{18}}$ constructed from Λ^0_{18} is shown in fig. 10.16. As indicated, it maps cells in Λ^0_{18} to the symbol 0 and walls (dislocations) to the symbol 1. Fig. 10.17 shows raw and filtered space-time plots of the evolution of a random initial condition under ECA 18.

In generating the filtered plot, the domain transducer is run over the spatial data in a particular direction: in our case, from left to right. This introduces a spatial

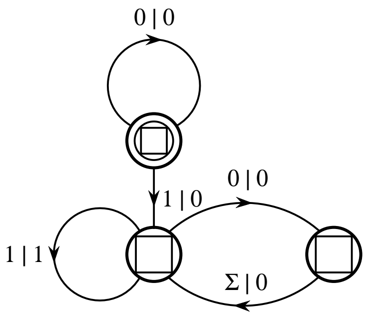

Fig. 10.16 Domain transducer $\mathrm{T}_{\Lambda^0_{18}}$ for domain Λ^0_{18} in ECA 18. This machine maps cells in Λ^0_{18} to the symbol 0 and dislocations to the symbol 1.

asymmetry into the picture. For example, the visible "jumps" to the right in the dislocation trajectories are due to the fact that as $\mathrm{T}_{\Lambda^0_{18}}$ is moved to the right over the data, it identifies a dislocation only by reading a 1 in the wrong place. That is, a 1 followed by an even number of consecutive 0s shows a dislocation at the right side, when the next 1 is encountered. More complicated transducers can be defined to evade this directionality. For example, the transducer could label all blocks $1(00)^n1, \quad n = 0, 1, 2, \ldots,$ as walls. With this detector, the dislocation becomes delocalized as it enters a triangle of 0s. The associated detector for bounding the delocalization region is more complex, requiring an infinite queue (first in first out, or FIFO) memory, if it is to not only recognize dislocations but also to label all participating sites appropriately. Because the filtered plot made with this tranducer is independent of the direction in which the transducer is passed over the data, this transducer is called a "symmetrized" domain transducer. Fig. 10.18 shows the same data as in fig. 10.17, filtered using the symmetrized domain transducer for domain Λ^0_{18}. Close comparison of figs. 10.17 and 10.18 shows that the asymmetric dislocation trajectories in the former follow the right edges of trajectories in the latter. Thus the two transducers simply provide different methods of visualizing the same phenomenon of dislocation motion.

There is in fact an entire cascade of nested domains in ECA 18. If we think of Λ^0_{18} as defined by the rule "every other site is arbitrary and the rest are zero", then these sublanguages are "every $\left(2^k\right)$th site is arbitrary and the rest are zero", assuming, of course, that $k > 0$. These are regular languages, which are denoted by $\Lambda^k_{18},\ k > 0$. Clearly $\Lambda^{k+1}_{18} \subset \Lambda^k_{18}$. For all positive k, Λ^k_{18} is a temporally periodic language orbit with period 2^{k-1}. Each language orbit

$$\left\{\mathbf{\Phi}_t\left(\Lambda^k_{18}\right) \ : \ 0 \le t < 2^{k-1},\ k > 0\right\} \tag{10.2}$$

is easily shown to be a temporally periodic domain. When the orbit recurs the origin is shifted by 2^{k-1} sites. As we will see in section 12.5, each of the Λ^k_{18} with $k > 0$ is unstable to perturbations within the larger set Λ^{k-1}_{18}.

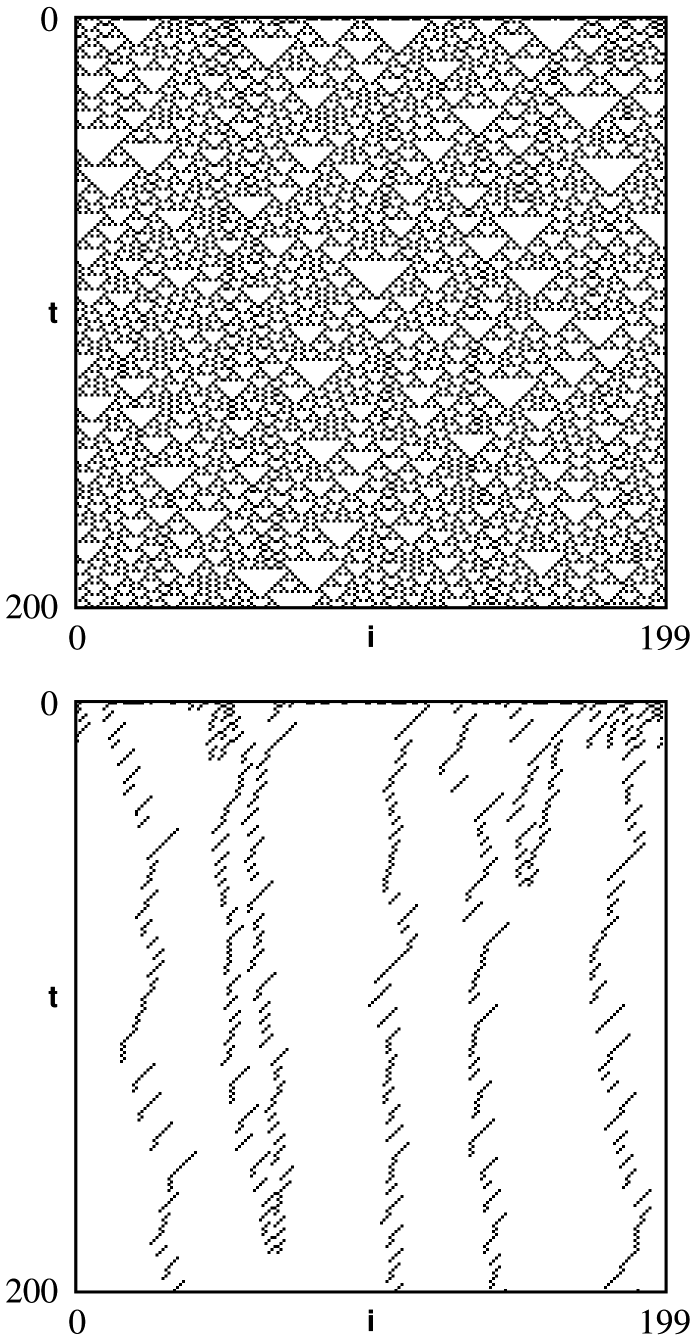

Fig. 10.17 Raw and filtered space-time plots of ECA 18, starting from a random initial condition and filtering with domain transducer $T_{\Lambda^0_{18}}$.

10.6 ECA 122

This is another rule with a chaotic domain, again found by machine reconstruction.

Proposition. Λ^0_{122}, illustrated in fig. 10.19, is a regular domain of ECA 122.

Proof: As before, temporal invariance was proved directly by the FME algorithm, and spatial homogeneity is evident from the process graph. ▌

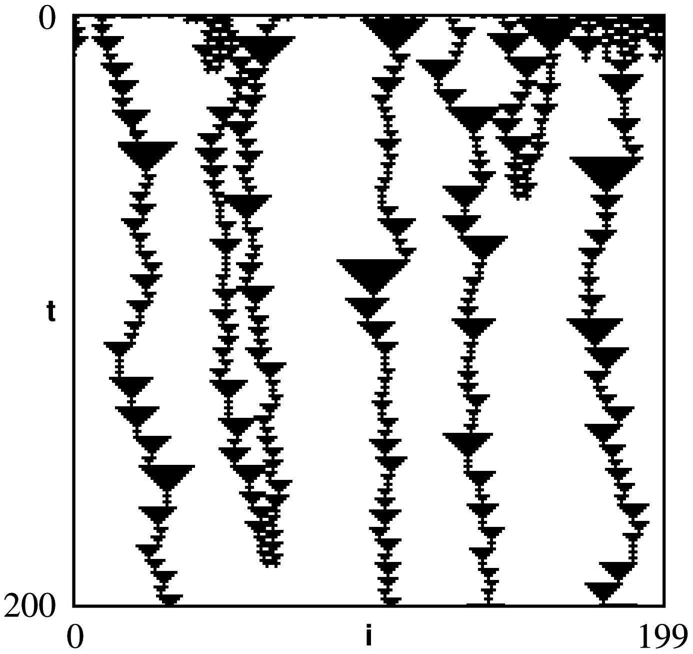

Fig. 10.18 Space time plot of ECA 18 using the symmetrized transducer described in the text. The raw data is the same as that shown in fig. 10.17.

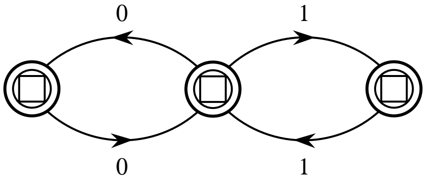

Fig. 10.19 Process graph of domain Λ^0_{122} in ECA 122.

In this case, the domain language consists of pairs of 0s and pairs of 1s, laid down at random. This means that all blocks of contiguous 0s or 1s in the domain must have even length. Thus a dislocation is indicated by a block of 0s or 1s with odd length.

The domain transducer $\mathrm{T}_{\Lambda^0_{122}}$ built from Λ^0_{122} is shown in fig. 10.20. As for ECA 18, this transduceris is run in a given direction over the data. When this is done, the first symbol *following* an odd-length block of 0s or 1s is identified as the dislocation. If the transducer reads from left to right, this is the cell to the right of the odd-length block; if the transducer moves from right to left, it is the cell to the left of the odd-lengh block.

A symmetrized version of this transducer marks all cells in odd-length blocks with 1s. Just as for the symmetrized domain transducer for Λ^0_{18}, this can be accomplished with a queue. Using the symmetrized transducer, we filtered the space-time plot of fig. 10.21(top), generated with ECA 122 from a random initial condition. The resulting filtered plot is shown in fig. 10.21(bottom).

Note the similarity of the filtered plots for ECA 18 and ECA 122 (figs. 10.18 and 10.21). In both cases, "delocalized" dislocations take the form of chains of triangles

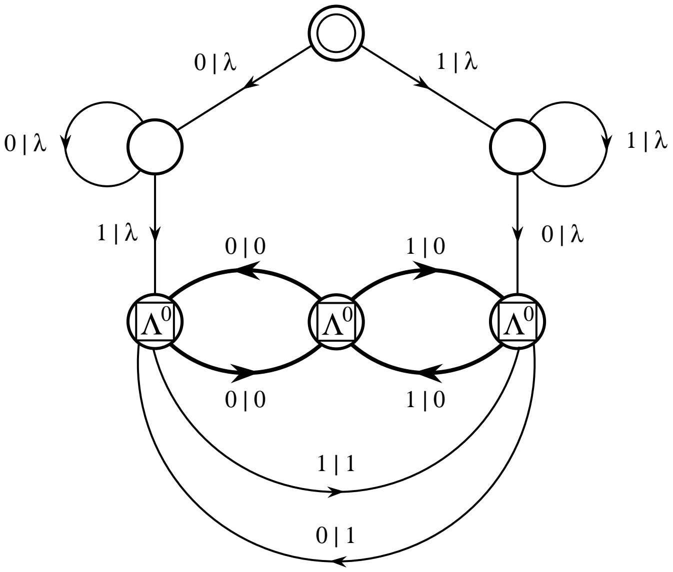

Fig. 10.20 ECA 122's domain transducer $\mathrm{T}_{\Lambda^0_{122}}$.

evolving against the domain, drifting at random to the left or right. In both cases, dislocations collide and annihilate in pairs. The filtered plots are strikingly similar, even though the domain patterns are notably different.

10.7 ECA 90

The domain structure of linear, "class 3" ECA 90 is particularly simple. The entire state space $\mathcal{A}^*$ is invariant under the rule, so that the largest domain is just $\Lambda^0_{90} = \mathcal{A}^*$. The domain transducer for this domain is therefore the nilpotent machine that maps all cells to 0. Just as for ECA 18, however, there are other domains embedded within in the state space. For example, the domain Λ^0_{18} of ECA 18 (fig. 10.14) is also a domain in ECA 90. However, the behavior of dislocations under the two rules is entirely different. As fig. 10.17 makes evident, an isolated dislocation in ECA 18 is preserved in time. In ECA 90, a pair of domains Λ^0_{18} separated by a single dislocation gives rise to an ever-expanding cascade of multiplying dislocations. This effect is shown clearly in fig. 10.22, which shows a space-time plot of an initial condition $\mathrm{s}_0 \in \Lambda^{0,0}_{18}$ consisting of two domains in Λ^0_{18} separated by a single dislocation, evolving under ECA 90. The unfiltered space-time data is shown on top; on the bottom is the same data filtered with ECA 18's domain transducer $\mathrm{T}_{\Lambda^0_{18}}$.

10.8 Dislocations in ECA 18

We continue the investigation of ECA 18 in this section on a deeper level by analyzing the motion of dislocations in the filtered space-time patterns. This type of analysis can be carried out for any CA in which the domains are known, and so this section is meant to be an indication of the general methods of investigating

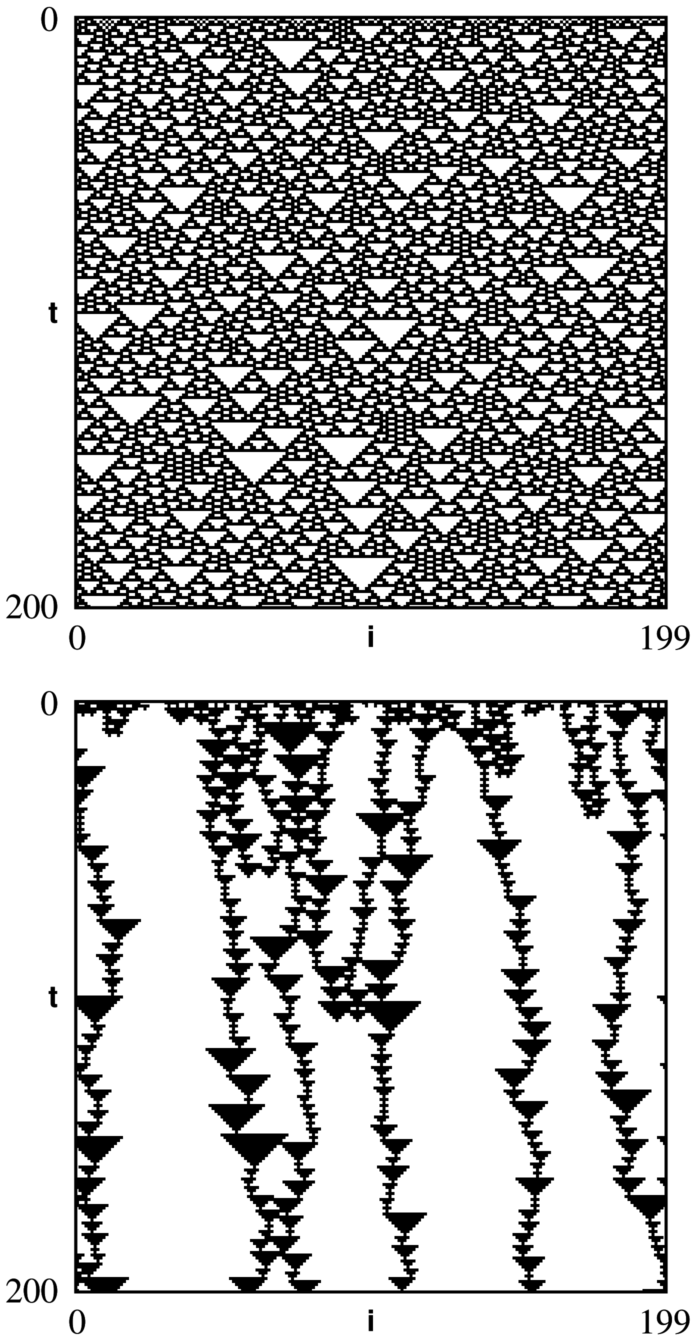

Fig. 10.21 Raw and filtered space-time plots of ECA 122, starting from a random initial condition.

domain boundaries in CA. Three different properties of dislocations in ECA 18 are studied here: (i) statistics of dislocations in ensembles of randomly chosen states; (ii) statististics of the motion of a single dislocation; and (iii) computational aspects of dislocation motion.

In the case of ECA 18, the walls have zero thickness: all spatial states s can be treated as concatenations of words $\omega \in \Lambda^0_{18}$ separated by dislocations. Then the